earthed). E is placed at the end of lever L and is elastically and electrically connected to the central part of the holder head.

The objective aperture and the decontaminator blade are placed below the straight broken line which has been drawn in Fig. 6(a) just above the bottom pole-piece face.

Both the standard specimen chamber and the basic x, y stage of the JEM 100 and 2000 series of microscopes are retained; the former is used for housing the additional drives needed to set and control the stage, and the latter for supporting the lifting and the tilting stages. A side-entry air lock is adopted for loading the specimen holder into the eucentric stage by means of a clamping jig, which is then withdrawn from the microscope.

Besides its application in tilting experiments, the stage will be useful in cases where both top and bottom surfaces of the specimen have to be investigated and, with little modification, for glancing-angle (reflection) microscopy (Cowley, 1988). In addition, provisions are made for the study of semiconductor devices by means of the electron beam induced current (EBIC) method, or for heating the sample. The present lens and stage features should also ease the incorporation of scanning tunneling facilities in a transmission electron microscope.

The development of the device is at a stage where detailed workshop drawings have been made and therefore its construction, even if complex, is feasible; it is however difficult to predict such uncertainties as mechanical instabilities. It is worthwhile to try to simplify further the mechanical solutions adopted, before proceeding to the construction of the eucentric tilting stage, in particular by attempting to incorporate piezoelectric elements in the design.

This research has been partly supported by Ministero Pubblica Istruzione, Rome.

References

COWLEY, J. M. (1988). *Reflection Electron Microscopy.* In *Surface and Interface Characterization by Electron Optical Methods*, edited by A. HOWIE & U. VALDRÈ. London: Plenum.

GENTY, B. (1972). In *Methodes et Techniques Nouvelles d'Observation en Métallurgie Physique*, p. 29. Paris: Societé Francaise de Microscopie Electronique.

MUNRO, E. (1975). A set of computer programs for calculating the properties of electron lenses. Rep. CUED/B-Elect TR45. Cambridge Univ. Engineering Department, Cambridge, England.

SPENCE, J. C. H. (1988). *Ultramicroscopy.* In the press.

TSUNO, K. & SMITH, K. C. A. (1986). *XIth Int. Congr. of Electron Microscopy, Kyoto*, 1986, Vol. I, pp. 295–296. Tokyo: Japanese Society of Electron Microscopy.

VALDRÈ, U. (1975). In *Electron Microscopy in Materials Science*, EUR 5515e, pp. 113–132. Luxembourg: Commission of the European Communities.

VALDRÈ, U. & TSUNO, K. (1986). *XIth Int. Congr. of Electron Microscopy, Kyoto*, 1986, Vol. II, pp. 925–926. Tokyo: Japanese Society of Electron Microscopy.

YANAKA, T. & WATANABE, M. (1966). *VIth Int. Congr. of Electron Microscopy, Kyoto*, 1966, Vol. I, pp. 141–142. Tokyo: Maruzen.

Acta Cryst. (1988). A**44**, 780–788

Results of Multislice Matrix Calculations for Convergent-Beam RHEED Patterns

BY ANDREW E. SMITH

Department of Physics, Monash University, Clayton, Victoria 3168, *Australia*

AND D. F. LYNCH

CSIRO, Division of Materials Science and Technology, Locked Bag 33, *Clayton, Victoria* 3168, *Australia*

(*Received* 30 *November* 1987; *accepted* 21 *March* 1988)

Abstract

Results of dynamical convergent-beam reflection high-energy electron diffraction (CBRHEED) calculations are presented for the (001) surface of magnesium oxide, the (111) surface of silicon and the (001) surface of molybdenum disulfide. These double rocking calculations are performed using a dynamical scattering approach. This is based on the evaluation of the surface parallel multislice matrix for the reflection (*i.e.* Bragg) geometry with account taken of the boundary conditions. Comparison with experimental results reported in the literature for these surfaces shows that only a full dynamical calculation with an appropriate number of beams is capable of a detailed description of the experimental contrast distributions. In particular, the nature of surface-wave-resonance effects is discussed.

1. Introduction

Though widely employed during the early years of electron diffraction (*e.g.* Finch, Quarrell & Wilman,

0108-7673/88/060780-09$03.00

1935; Goodman, 1981), reflection high-energy electron diffraction (RHEED) has re-emerged during the past few years as a most useful diagnostic tool with particular use in the monitoring of surface structure during crystal growth by molecular-beam epitaxy (Neave, Joyce, Dobson & Norton, 1983). Various experimental methods have concentrated on extending RHEED to improve the information content of the diffraction pattern. One such technique has been termed convergent-beam RHEED (CBRHEED) as it is analogous to the convergent-beam (CB) technique used in transmission electron diffraction and microscopy (*e.g.* Goodman, 1972; Steeds, 1979).

CBRHEED effects have been investigated in both specially built diffraction cameras (Ichimiya, Kambe & Lehmpfuhl, 1980; Lehmpfuhl & Dowell, 1986) and in modern commercial microscopes (Shannon, Eades, Meichle & Turner, 1985; Peng & Cowley, 1987). It is the object of the present paper to report dynamically calculated CBRHEED patterns obtained by a surface parallel multislice method. This calculation scheme, which is based on a surface diffraction scheme proposed by Lynch & Moodie (1972), is founded on many of the concepts of Cowley & Moodie's (1957) multislice method. It is quite similar to that used for standard RHEED spectra by Maksym & Beeby (1981). The calculated patterns of the present work allow direct comparison with experimental measurements on magnesium oxide and molybdenum disulfide reported by Shannon *et al.* (1985) together with those on silicon by Lehmpfuhl & Dowell (1986).

In previous work, other authors have discussed CBRHEED in terms of surface-resonance arguments (Ichimiya, Kambe & Lehmpfuhl 1980; Lehmpfuhl & Dowell, 1986; Peng & Cowley, 1987) and also by a combination of kinematical and symmetry ideas (Shannon, Eades, Meichle, Turner & Buxton, 1984; Shannon *et al.*, 1985). Whilst some of the overall features are explicable by simple geometrical and Bragg's-law arguments, the present work demonstrates that a full dynamical calculation with appropriate boundary conditions and an appropriate number of beams describes more fully the experimental contrast distributions. As a corollary it thus allows the application of appropriate geometrical arguments with more confidence.

2. The CBRHEED geometry

High-energy electron diffraction from crystal surfaces is most commonly envisaged by employing the Ewald-sphere construction. The various possible diffracted directions are then represented by a series of points which mark the intersections of the sphere with the reciprocal-lattice rods of the crystal surface. The rods, which correspond to the reciprocal-lattice points of the three-dimensional bulk crystal, are to be considered non-uniform because of the crystal structure normal to the surface.

In standard RHEED an ideal incident beam consists of parallel plane waves. However, in the CBRHEED experiment the incoming beam is deliberately chosen to have a range of allowed incident angles up to some maximum convergence angle, as defined by a limiting aperture (see Fig. 1). The series of spots and streaks seen in an ordinary RHEED diffraction pattern can be immediately understood in terms of the intersection of the Ewald sphere with the rods, together with experimental resolution effects. On the other hand, a CBRHEED pattern is more complicated since spots are produced for each of the many allowed incident directions. However, as long as the aperture size is small enough, the patterns for the individual rods are separated.

Owing to the effect of the surface boundary condition, the reflection geometry produces a distortion of the beam envelopes in CBRHEED which is not present in the transmission case (Shannon *et al.*, 1984). Though all of the other various diffracted beams are affected, the specular reflected beam in particular does retain the initial disk form. For the case of beam incidence close to a zone axis of the crystal, it is possible to determine the diffracted beam envelopes geometrically for each member of the corresponding row of reciprocal-lattice rods (Shannon *et al.*, 1985; Smith & Lynch, 1987*a*).

In the geometrical interpretation of CBRHEED patterns it can be useful to remember a further point concerning the nature of the reflection (Bragg) geometry. This implies that the loci of the Kikuchi bands parallel to the surface correspond exactly to the position of the elastically scattered Bragg reflections of the same index.

3. CBRHEED calculations

(*a*) *Computational schemes*

The interaction strength between electrons and crystalline material requires that RHEED calculations should in general be performed using dynamical schemes. The elastic scattering intensities can be determined by the solution of the dynamical diffraction problem expressible as the coupling between N beams. This then leads to the solution of a quadratic $N \times N$ matrix problem. In the case of transmission

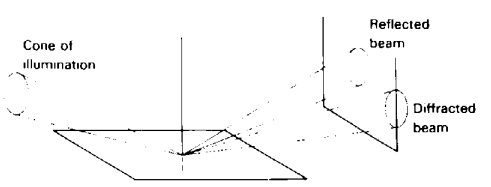

Fig. 1. Schematic diagram of the CBRHEED experiment.

diffraction (Laue geometry) at high energy, great simplification results by ignoring the N backward eigenvalues out of the total $2N$ eigenvalues corresponding to both forward and backward travelling waves (*e.g.* Cowley, 1981). However, for the reflection geometry, one should, in principle, solve the full $2N$ eigenvalue problem. Moon (1972) and Colella (Colella, 1972; Colella & Menadue, 1972) employed different dynamical computation schemes to treat the simple 'systematics' case, namely the incorporation of reciprocal-lattice points on one particular lattice rod.

Much fuller elastic RHEED calculations were carried out by Maksym & Beeby (1981) and independently by Ichimiya (1983, 1985). These authors utilized a multislice formulation of the problem (Cowley & Moodie, 1957). In effect, transfer matrix solutions were found after determination for each slice of the two-dimensional Fourier components followed by solution using different matrix manipulation techniques. These formulations of the multislice computation method for the reflection geometry turn out to be equivalent to a low-energy electron diffraction (LEED) calculation scheme proposed by Lynch & Moodie (1972). The generalized expressions for this approach have been published separately (Lynch & Smith, 1983) and are the basis of the computer codes used in the present work.

(*b*) *Computational parameters*

To determine suitable computational parameters, one may divide the problem in a somewhat arbitrary way as determination of: (1) slice thickness; (2) total crystal thickness; and (3) truncation in number of rods.

Consider initially the slice thickness. Although it may be possible in transmission multislice calculations to take slice thicknesses to be of the order of an individual unit cell, for the reflection calculation one must necessarily expect this distance to be less than of the order of one tenth of a unit cell, as the contributing lattice vectors are of order ten. This follows from the necessity of back-scattered electrons to cross the crystal-surface/vacuum interface, which traps the low-order reflections by the inner potential (refractive-index effect). Ichimiya (1983) came to the same order-of-magnitude conclusion by a combined shape transform and Debye–Waller argument. In the present computations, slice thickness was checked by decreasing thickness until convergence was reached.

The second parameter, *i.e.* the total crystal thickness, is closely related to the assignment of absorption potential value which takes care of the effects of inelastic scattering in a somewhat semi-empirical way. For the accelerating voltages of the present work, values for the absorption potential in the range 0·1–−1 eV are indicated by transmission experiments and calculations (*e.g.* Goodman & Lehmpfuhl, 1967; Radi, 1970; Voss, Lehmpfuhl & Smith, 1980). We have adopted values in this range; computational convergence in total crystal thickness is then achieved for the present work using a layer doubling scheme in the region of 10 nm. This is in agreement with computations by Maksym & Beeby (1981) and Ichimiya (1983).

Finally, for reasons of computational efficiency a choice must be made regarding those rods to be included in the calculation. This is made by establishing, for the different angles of incidence, which rods are closest to the Ewald sphere (modified by the crystal potential). In our calculation we include both propagating and attenuating waves, corresponding to the interior and exterior of the sphere respectively. The effect of changing the number of rods in the calculation is one of the points illustrated and discussed in the following sections.

4. Summary of matrix multislice method and choice of parameters for magnesium oxide, silicon (111) and molybdenum disulfide

CBRHEED calculations were performed in the present work for magnesium oxide, silicon and molybdenum disulfide by means of a computation based on the scattering-matrix approach of Lynch & Moodie (1972) to describe the dynamical scattering effects. This method combines the multislice treatment of electron scattering in a crystal (Cowley & Moodie, 1957), with Tournarie's (1962) supermatrix formulation. The full expressions for the general case are presented by Lynch & Smith (1983). The unit-cell parameters for the three materials were taken from Wyckoff (1963). The scattering matrices were then constructed using scattering factors for neutral atoms from Doyle & Turner (1968).

As a first approximation, the surface was in all three cases represented as an abrupt termination of the bulk structure. Such an assumption is well supported for the cases of magnesium oxide and molybdenum disulfide by LEED results as they indicate very little change in the spacing of the topmost layer. For molybdenum disulfide, see Mrstik, Tong, Kaplan & Ganguly (1975) and Mrstik, Kaplan, Reinecke, Van Hove & Tong (1977); for magnesium oxide, see Kinniburgh (1975, 1976) and Welton-Cook & Berndt (1982). A similar conclusion for magnesium oxide was reached by Maksym (1985), who used a dynamical RHEED calculation at 10 keV incident energy to analyse experimental data by Ichimiya & Takeuchi (1983). For silicon (111) the assumption is to be regarded merely as preliminary, as the reordering of the Si (111) surface is a complex problem that has been closely studied with varying interpretations through a period of over twenty years. Particular mention might be given to the contribution of the Tokyo Institute of Technology group (*e.g.* Yagi,

Takayanagi & Honjo, 1982; Takayanagi, Tanishiro, Takahashi & Takahashi, 1985). However, for the present work Ino's (1977) RHEED results suggest that the simple initial choice of the diamond lattice might well be an appropriate starting point for an analysis of Lehmpfuhl & Dowell's (1986) results considering the crystal preparation that was employed.

Initial calculations employed the value of the zeroth-order Fourier component of the potential $V(0, 0, 0)$, *i.e.* the inner potential, obtained directly from superposition of the atoms. This parameter was varied by several eV, but very little change in calculated pattern resulted as refractive-index effects dominate for smaller grazing angles than those employed in the experiments under consideration. For the patterns shown in Figs. 2 to 4, an inner potential value of 14·3 eV (Turner & Cowley, 1981, quoting Cowley, Goodman & Rees, 1957) was taken for magnesium oxide (*cf.* superposition value 17·7 eV). For Figs. 5 and 7–12 the superposition values of 13·8 and 16·8 eV were taken for silicon and molybdenum disulfide respectively.

For the three materials under consideration, a uniform imaginary potential was adopted. For the case of magnesium oxide a value of 0·1 eV was used, as guided by transmission work (*cf.* Goodman & Lehmpfuhl, 1967; Radi, 1970) and this value was also adopted for molybdenum disulfide. However, for the case of silicon a larger value of 0·7 eV was used, again as indicated by transmission work (*cf.* Voss, Lehmpfuhl & Smith, 1980).

Magnesium oxide is a member of the sodium chloride family, and accordingly, in order to eliminate redundant beams, a unit cell with volume one half of the conventional cell can be chosen. This cell is obtained by a 45° rotation in the xy plane together with a corresponding length reduction by the factor $1/\sqrt{2}$. Similarly one may also reduce the calculation size for incidence on the (111) face of diamond-lattice silicon. This may be achieved by adopting a smaller unit cell which consists of hexagonal a and b axes in the surface with unit-cell lengths equal to $1/\sqrt{2}$ of the conventional cell side. In addition a perpendicular c axis is employed with corresponding cell length equal to $\sqrt{3}$ of the conventional cell side. In contradistinction, the various diffraction calculations were performed on molybdenum disulfide using conventional cells.

5. Results

(*a*) *Magnesium oxide*

Figs. 2–4 illustrate the results of the dynamical calculation for magnesium oxide. Calculations were performed on a 41×41 rectangular mesh and show, in particular, the effect of changing the number of rods included in the calculation. Fig. 2 shows the result of including only the specular rod [equivalent to the 'systematics' simplification of Moon (1972) and Colella & Menadue (1972)]. A horizontal band of intensity corresponding to the 008 reflection is the only feature seen across Fig. 2 because of cylindrical symmetry. The effect of including the $(\bar{1}\bar{1})$ and (11) rods is then seen in Fig. 3. However, the full effect of dynamical coupling is first seen by the further inclusion of the $(\bar{2}\bar{2})$ and (22) rods to give a full five-rod calculation as displayed in Fig. 4. Further inclusion of more rods gives no effect as they are too

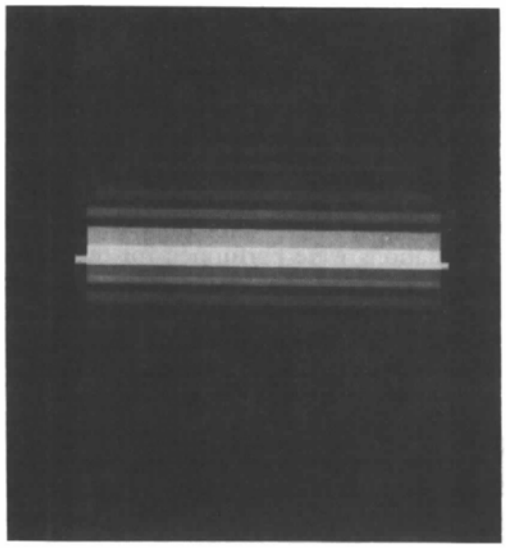

Fig. 2. Results of dynamical CBRHEED calculations for the (00) specular rod with incidence close to the ⟨100⟩ zone axis in magnesium oxide at 40 keV incident energy. The angle of incidence at the centre of the circular disk defining the pattern circumference is 3° corresponding to $3{\cdot}75c^*$ reciprocal-lattice vectors. The aperture radius is 0·6° corresponding to one half of the reciprocal-lattice rod spacing. The calculation is carried out on a 41×41 rectangular mesh with inner potential equal to 14·3 eV and absorption potential equal to 0·1 eV.

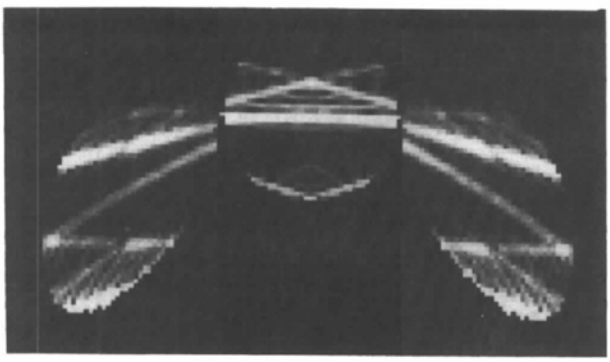

Fig. 3. Results of dynamical CBRHEED calculations for three rods comprising the (00) specular together with the $(\bar{1}\bar{1})$ and (11) non-speculars with incidence close to the ⟨100⟩ zone axis in magnesium oxide at 40 keV incident energy. Other computational parameters as in Fig. 2.

far away from the Ewald sphere to couple strongly. Fig. 4 compares most favourably with the experimental pattern reported by Shannon *et al.* (1985).

(*b*) *Silicon* (111)

Results of the calculation are shown for Si (111) in Fig. 5 which displays computations on a 41×41 hexagonal mesh. Illustrated is the circular disk corresponding to the specular rod (00) reflection. Also shown are portions of the lobe shapes corresponding to the non-specular $(\bar{1}\bar{1})$ and (11) rods which are above the crystal edge. The angle of incidence at the centre of the circular disk defining the pattern circumference is 1·3° corresponding to five c^* reciprocal-lattice vectors. The aperture radius is 0·8° corresponding to the reciprocal-lattice rod spacing. Since this geometry results in partial overlap of the central disk by the side lobes, for the sake of clarity the non-specular patterns have been displaced horizontally. The calculations were performed for the three rods closest to the Ewald sphere. The smallest grazing angles of incidence correspond to non-emergence of the non-specular $(\bar{1}\bar{1})$ and (11) rods. Accordingly, the lower parts of the (00) beam disk are strongly influenced by surface-resonance conditions in respectively the $(\bar{1}\bar{1})$ and (11) rods. An increase in the number of rods achieved no noticeable change in the pattern, whilst a decrease in number to one rod produced a cylindrically symmetric pattern similar to that shown for magnesium oxide in Fig. 2. If one allows for a slight amount of overlap in the experimental pattern, the central disk together with the non-specular wings of Fig. 5 reproduce most faithfully the main features of the corresponding experimental pattern reported by Lehmpfuhl & Dowell (1986) as their Fig. 6.

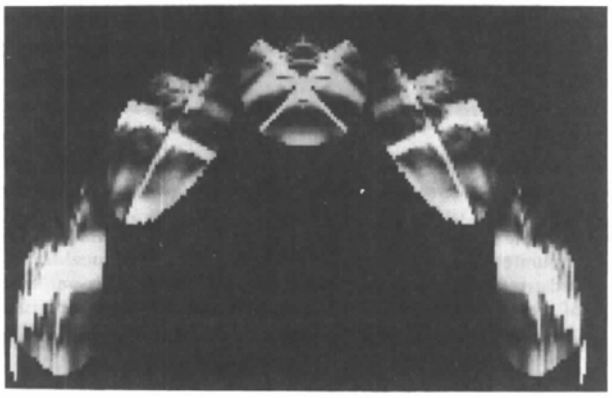

Fig. 4. Results of dynamical CBRHEED calculations for five rods comprising the (00) specular together with the $(\bar{2}\bar{2})$, $(\bar{1}\bar{1})$, (11) and (22) non-speculars with incidence close to the ⟨100⟩ zone axis in magnesium oxide at 40 keV incident energy. Other computational parameters as in Fig. 2.

Fig. 5. Results of dynamical CBRHEED calculations for three rods comprising the (00) specular together with the $(\bar{1}\bar{1})$, and (11) non-speculars for incidence close to the $\langle 11\bar{2} \rangle$ azimuth for the silicon (111) surface at 80 keV incident energy.

(*c*) *Molybdenum disulfide*

We have recently repeated some of Shannon *et al.*'s experimental measurements on molybdenum disulfide to gain experience in the CBRHEED technique in order to continue our work on the surface characterization of the layered transition-metal dichalcogenides (Smith & Lynch, 1987*b*). Crystals of the natural mineral molybdenite (molybdenum disulfide) were mounted in special copper holders which could hold the crystal with the surface plane nearly parallel to the optical axis of a Philips 420 electron microscope. The crystals were mounted in the holders and then were cleaved in air just prior to insertion in the electron microscope. Fig. 6 shows results of one of our measurements. Though the patterns are preliminary and in particular are not as precisely aligned as Shannon *et al.*'s symmetric result, they do show the shadow edge of the crystal surface, which is not included in their published pattern [Fig. 5 of Shannon *et al.* (1985)]. The angle of incidence in our pattern is clearly tilted by approximately one quarter of a reciprocal-lattice vector away from the exact symmetric condition. This tilt is such that the right-hand edge of the central-beam disk corresponds to the centre of the calculated central-beam disk in Fig. 9 (see below). Fig. 6(*a*) is a normal CBRHEED exposure, (*b*) is a longer exposure to bring out the Kikuchi bands and surface shadow, whilst (*c*) is taken for an even longer exposure and shows HOLZ (higher-order Laue zone) effects in the CBRHEED pattern for molybdenum disulfide (Eades, Smith & Lynch, 1987; Eaglesham, 1987).

For the case of molybdenum disulfide we again reproduce a series of calculated patterns that demonstrate the effect of increasing the number of rods. Molybdenum disulfide has a unit-cell length of 12·295 Å in its most common $2H$ form, which consists of two-layer sandwiches with hexagonal symmetry. The correspondingly small c^* spacing might be expected to provide a great amount of diffraction structure as many different beams can be brought into play. In particular, as discussed in this section, it affords the unequivocal demonstration of a surface-wave resonance effect (Miyake & Hayakawa, 1970; McRae, 1979). This condition obtains when incidence is such

that a reciprocal-lattice rod is tangent to the Ewald sphere.

In addition, results of calculations will also be shown for the less-common $3R$ polytype of molybdenum disulfide which is found in some crystal samples. This structure has a unit cell which comprises three-layer sandwiches with rhombohedral symmetry. This polytype is made up of the same basic single sandwiches of S–Mo–S ordered in a different stacking sequence but with the same basic interlayer spacing. Comparison of patterns has a bearing on possible effects from surface steps and stacking faults in CBRHEED patterns.

(*a*)

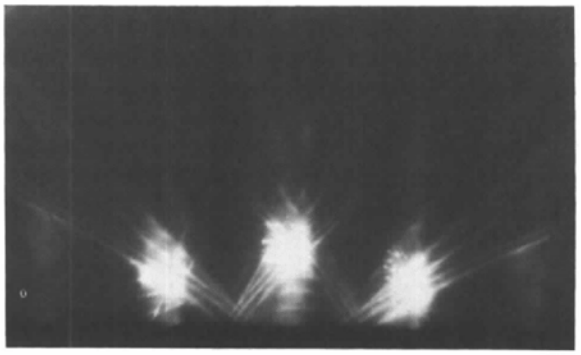

(*b*)

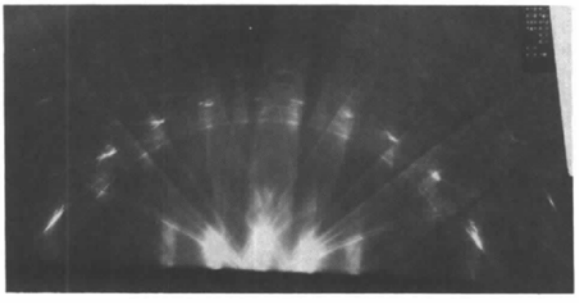

(*c*)

Fig. 6. Experimental CBRHEED patterns recorded near to the $\langle 11\bar{2}0\rangle$ zone axis of molybdenum disulfide at 100 keV. (*a*) Normal exposure showing the $(\bar{1}\bar{1})$, (00) and (11) rods. (*b*) Longer exposures demonstrating the shadow edge of the crystal and some Kikuchi bands. (*c*) Longest exposure, with smaller print magnification, showing more clearly the shadow edge of the crystal as well as the occurrence of the HOLZ reflections.

The sequence of Figs. 7 to 9 shows results at one angle of incidence with different numbers of calculation rods for molybdenum disulfide with the $2H$ structure. This is the polytype most commonly found in both natural crystals and those grown in the laboratory (Trigunayat & Verma, 1976). In all cases calculations were performed on a 121×121 hexagonal mesh. Fig. 7 shows the 'barber's pole' result for inclusion of only the specular rod. The larger number of

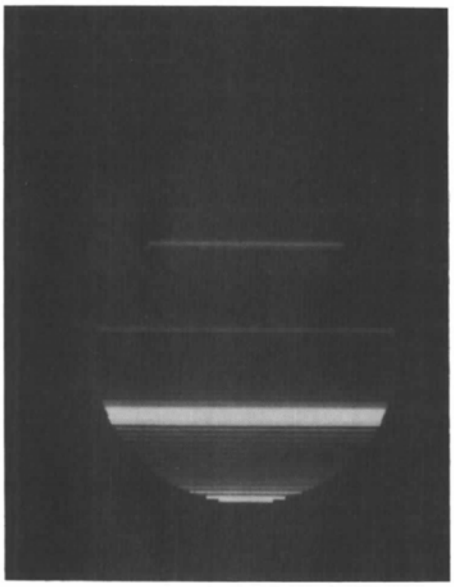

Fig. 7. Results of dynamical CBRHEED calculations for the (00) specular rod with incidence close to the $\langle 11\bar{2}0\rangle$ zone axis in molybdenum disulfide for the $2H$ structure at 100 keV incident energy. The angle of incidence at the centre of the circular disk defining the pattern circumference is 2·42° corresponding to $14c^*$ reciprocal-lattice vectors. The aperture radius is 0·34° corresponding to 0·4 of the reciprocal-lattice rod spacing. The calculation is carried out on a 121×121 hexagonal mesh with inner potential equal to 16·8 eV and absorption potential equal to 0·1 eV.

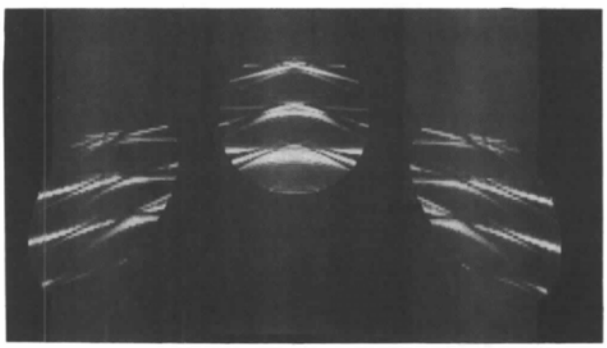

Fig. 8. Results of dynamical CBRHEED calculations for three rods comprising the (00) specular together with the $(\bar{1}\bar{1})$ and (11) non-speculars with incidence close to the $\langle 11\bar{2}0\rangle$ zone axis in molybdenum disulfide for the $2H$ structure at 100 keV incident energy. Other computational parameters as in Fig. 7.

horizontal bars than in Fig. 2 is of course directly related to the smaller c^* unit-cell axis. Fig. 8 demonstrates the effect of including the $(\bar{1}\bar{1})$ and (11) rods, whilst Fig. 9 shows a five-rod calculation which further includes the $(\bar{2}\bar{2})$ and (22) rods. Comparing in particular Figs. 8 and 9 one notes that there is very little difference in the lower half of the specular disk, corresponding to the lower two c^* reflections visible in Fig. 7. However for the second highest c^* reflection, there are two tilted traces present in Fig. 9 that cannot be seen in Fig. 8. These traces can be related to emergence conditions for the outer non-specular beams (*i.e.* surface resonance). In a similar way corresponding traces, though somewhat distorted, can be seen for equivalent positions in the inner non-specular patterns when comparing Figs. 8 and 9. For the highest c^* reflection in the specular disk, when compared with Fig. 8, one extra pair of traces can be seen to cross in Fig. 9. This can also be ascribed to the emergence condition as this part of the pattern corresponds to a higher angle of incidence and it is therefore 'easier' for the corresponding outer non-specular beam to emerge. There is also a small amount of additional structure for the highest c^* reflection in the specular disk that can be seen in Fig. 9 but not in Fig. 8, with corresponding structure in the inner non-specular patterns.

The general form of the calculated pattern displayed in Fig. 9 is in fairly good agreement with the experimental pattern of Shannon *et al.* and also the present work (Fig. 6). It might perhaps be emphasized that the basic form of the patterns is given by the c^* spacing, which is well known for the structure. However, as this quantity is rather small, certainly when compared with the other materials considered in this paper, the possibility of a small change in angle of incidence becomes pertinent. Accordingly, Fig. 10 shows a CBRHEED calculated pattern for the $2H$ molybdenum disulfide structure at a slightly higher angle of incidence than in Fig. 9. This was chosen such that the various c^* reflections appear to be moved down approximately one in the sequence of horizontal bands. One immediately notices that the highest c^* reflection in the specular disk in Fig. 10 is rather weak (as is indeed the next reflection further up in the sequence, though this is not shown in the present work). This weakness can be related to a small Fourier coefficient for the $2H$ molybdenum disulfide structure. This particular portion of the pattern would in itself indicate that the incidence conditions of Fig. 9 match more closely those of the experimental results than do those of Fig. 10.

The third horizontal bar from the top of the central disk in the calculated pattern of Fig. 9 shows a three-fold splitting which is not evident in the experiment. Thus it was decided to repeat the calculations for the $3R$ molybdenum disulfide structure. Fig. 11 shows the result of a five-rod calculation with the same angle of incidence as in Fig. 9, whilst Fig. 12 stands in the same correspondence to Fig. 10.

Comparing results for the $2H$ and $3R$ structures, one sees, as might be expected, that the CBRHEED calculated patterns look rather alike. This may be readily appreciated because, although the stacking sequence is different in the two structures, the layer spacing is the same and thus the position of the horizontal bars in the patterns is identical. One particular feature that may be commented upon in Fig. 12 is the relative strength of the uppermost c^* reflection.

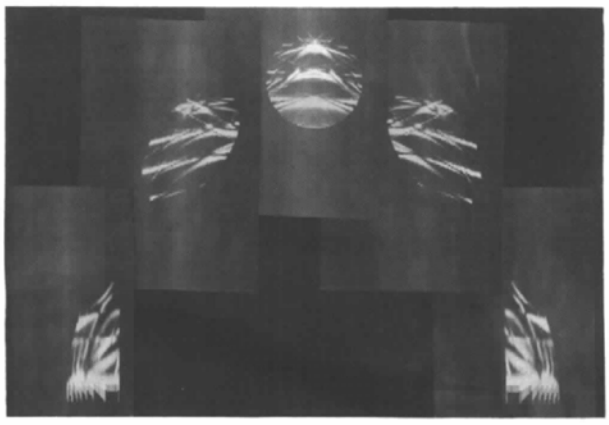

Fig. 9. Results of dynamical CBRHEED calculations for five rods comprising the (00) specular together with the $(\bar{2}\bar{2})$, $(\bar{1}\bar{1})$, (11) and (22) non-speculars with incidence close to the $\langle 11\bar{2}0\rangle$ zone axis in molybdenum disulfide for the $2H$ structure at 100 keV incident energy. Other computational parameters as in Fig. 7.

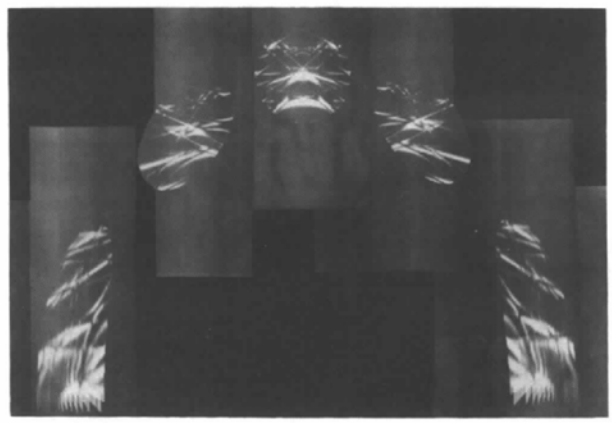

Fig. 10. Results of dynamical CBRHEED calculations for five rods comprising the (00) specular together with the $(\bar{2}\bar{2})$, $(\bar{1}\bar{1})$, (11) and (22) non-speculars with incidence close to the $\langle 11\bar{2}0\rangle$ zone axis in molybdenum disulfide for the $2H$ structure at 100 keV incident energy. The angle of incidence at the centre of the circular disk defining the pattern circumference is 2·63° corresponding to 15·25c^* reciprocal-lattice vectors. The aperture radius is 0·34° corresponding to 0·4 of the reciprocal-lattice rod spacing. Other computational parameters as in Fig. 7.

From the amount of CBRHEED experimental data available it is difficult to distinguish between the two polytypes. It is clear that for a given crystal surface a minimum measurement requires the recording of patterns over an angular range corresponding to both Figs. 9 and 10.

The position of the shadow edge of the crystal surface is of particular importance for the comparison between calculation and experiment as it indicates that the incidence conditions of Figs. 9 and 11 more closely match the experiment than those of Figs. 10 and 12. Indeed, one is not able to ascertain any intensity for the outer non-specular beams in the experimental patterns in either Fig. 6 of the present work or in the experimental pattern of Shannon *et al.* However, it is possible to argue that the height of features above the shadow edge of the outer non-speculars in Figs. 9 and 11 is such that these beams might easily be blocked by only a small amount of roughness present on the crystal surface. It would require a much larger effect to block out the corresponding regions of Figs. 10 and 12.

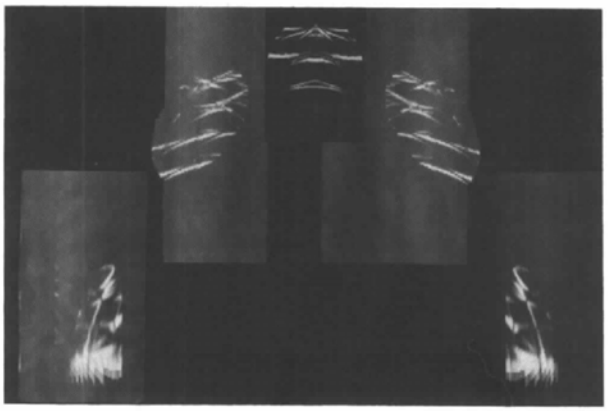

Fig. 11. Results of dynamical CBRHEED calculations for five rods comprising the (00) specular together with the $(\bar{2}\bar{2})$, $(\bar{1}\bar{1})$, (11) and (22) non-speculars with incidence close to the $\langle 11\bar{2}0\rangle$ zone axis in molybdenum disulfide for the $3R$ structure at 100 keV incident energy. The angle of incidence at the centre of the circular disk defining the pattern circumference is 2·4° corresponding to $21c^*$ reciprocal-lattice vectors. The aperture radius is 0·34° corresponding to 0·4 of the reciprocal-lattice rod spacing. Other computational parameters as in Fig. 7.

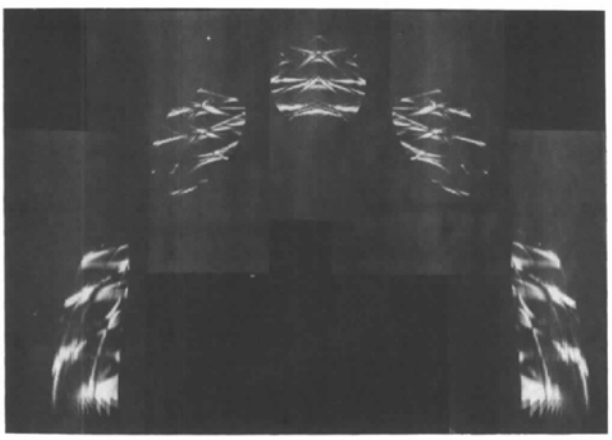

Fig. 12. Results of dynamical CBRHEED calculations for five rods comprising the (00) specular together with the $(\bar{2}\bar{2})$, $(\bar{1}\bar{1})$, (11) and (22) non-speculars with incidence close to the $\langle 11\bar{2}0\rangle$ zone axis in molybdenum disulfide for the $3R$ structure at 100 keV incident energy. The angle of incidence at the centre of the circular disk defining the pattern circumference is 2·63° corresponding to $22{\cdot}875c^*$ reciprocal-lattice vectors. The aperture radius is 0·34° corresponding to 0·4 of the reciprocal-lattice rod spacing. Other computational parameters as in Fig. 7.

Though comparisons have been made in this section of structures with different stacking sequences, these considerations still leave unanswered the detailed results of a defect in layer stacking due to cleavage between layers at a non-integral number of unit cells, an occurrence quite likely in the neighbourhood of a surface step.

Concluding remarks

Results from dynamical CBRHEED calculations are able to simulate most of the structure and intensities seen in the corresponding experimental patterns for magnesium oxide, silicon (111) and molybdenum disulfide. There are, however, some disagreements, particularly for the outermost non-specular parts of the patterns where effects such as surface roughness and the precise form of the crystal surface potential play a particularly important part. Surface resonance effects are clearly present in this technique. However, it is the combination of this process with all the other dynamical scattering processes which determines the final form of the observed results.

Whilst some of the disagreement between theory and experiment can be attributed to inelastic scattering and electron optics effects (particularly at low angles), there might also be a contribution from surface structure. Surface steps and stacking faults in particular are expected to occur in molybdenum disulfide. Furthermore, they are sometimes related to interfacial regions of the different polytypes (Amelinckx & Delavignette, 1962; Steeds, Tatlock & Hampson, 1973; Tatlock & Steeds, 1973; Goodman, 1974). There have been two successful methods in dealing with surface steps in RHEED calculations. One of these has been by means of a periodic assembly of steps (Kawamura & Maksym, 1985). The alternative, though fundamentally equivalent method, is to slice perpendicular to the crystal surface and apply the principle of periodic continuation (Peng & Cowley, 1986). This latter method has the advantage of more explicit use of the forward-scattering approximation. Both methods are being introduced into the CBRHEED computational scheme used in the present study.

We thank Dr Alex Moodie for his considerable help and friendly advice in the understanding of dynamical electron diffraction from surfaces. We also express our gratitude to Dr Alwyn Eades for his major advice and assistance in the methods necessary to record CBRHEED experimental results using a Philips 420 electron microscope. We also express our thanks to Dr W. Birch of the State Museum of Victoria for the donation of a crystal of molybdenite. The project has been supported by a CSIRO/Monash University Collaborative Research Grant. AES acknowledges assistance from the Monash University Vice-Chancellor's Special Research Fund Advisory Committee.

References

AMELINCKX, S. & DELAVIGNETTE, P. (1962). *Dislocations in Layer Structures*, in *Direct Observation of Imperfections in Crystals*, edited by J. B. NEWKIRK & J. H. WERNICK. New York: Interscience.

COLELLA, R. (1972). *Acta Cryst.* A**28**, 11-15.

COLELLA, R. & MENADUE, J. F. (1972). *Acta Cryst.* A**28**, 16-22.

COWLEY, J. M. (1981). *Diffraction Physics*, 2nd ed. Amsterdam: North-Holland.

COWLEY, J. M., GOODMAN, P. & REES, A. L. G. (1957). *Acta Cryst.* **10**, 19-25.

COWLEY, J. M. & MOODIE, A. F. (1957). *Acta Cryst.* **10**, 609-619.

DOYLE, P. A. & TURNER, P. S. (1968). *Acta Cryst.* A**24**, 390-397.

EADES, J. A., SMITH, A. E. & LYNCH, D. F. (1987). In *Proc. 45th Annual Meeting Electron Microscopy Society of America*, edited by G. W. BAILEY, p. 30. San Francisco Press.

EAGLESHAM, D. J. (1987). Program Abstract: *HOLZ Effects in Convergent-Beam RHEED*, in Nato Advanced Research Workshop on RHEED and Reflection Imaging of Surfaces, Veldhoven, The Netherlands. (Unpublished.)

FINCH, G. I., QUARRELL, A. G. & WILMAN, H. (1935). *Trans. Faraday Soc.* **31**, 1051-1080.

GOODMAN, P. (1972). *Acta Cryst.* A**28**, 92-93.

GOODMAN, P. (1974). *Nature (London)*, **251**, 698-702.

GOODMAN, P. (1981). Editor. *Fifty Years of Electron Diffraction.* Dordrecht: Reidel.

GOODMAN, P. & LEHMPFUHL, G. (1967). *Acta Cryst.* **22**, 14-24.

ICHIMIYA, A. (1983). *Jpn. J. Appl. Phys.* **22**, 176-180.

ICHIMIYA, A. (1985). *Jpn. J. Appl. Phys.* **24**, 1365.

ICHIMIYA, A., KAMBE, K. & LEHMPFUHL, G. (1980). *J. Phys. Soc. Jpn*, **49**, 684-688.

ICHIMIYA, A. & TAKEUCHI, Y. (1983). *Surf. Sci.* **128**, 343-349.

INO, S. (1977). *Jpn. J. Appl. Phys.* **16**, 891-908.

KAWAMURA, T. & MAKSYM, P. A. (1985). *Surf. Sci.* **161**, 12-24.

KINNIBURGH, C. G. (1975). *J. Phys. C*, **8**, 2382-2394.

KINNIBURGH, C. G. (1976). *J. Phys. C*, **9**, 2695-2708.

LEHMPFUHL, G. & DOWELL, W. C. T. (1986). *Acta Cryst.* A**42**, 569-577.

LYNCH, D. F. & MOODIE, A. F. (1972). *Surf. Sci.* **32**, 422-438.

LYNCH, D. F. & SMITH, A. E. (1983). *Phys. Status Solidi B*, **119**, 355-361.

MAKSYM, P. A. (1985). *Surf. Sci.* **149**, 157-174.

MAKSYM, P. A. & BEEBY, J. L. (1981). *Surf. Sci.* **110**, 423-438.

MCRAE, E. G. (1979). *Rev. Mod. Phys.* **51**, 541-568.

MIYAKE, S. & HAYAKAWA, K. (1970). *Acta Cryst.* A**26**, 60-70.

MOON, A. R. (1972). *Z. Naturforsch. Teil A*, **27**, 390-395.

MRSTIK, R., KAPLAN, R., REINECKE, T. L., VAN HOVE, M. & TONG, S. Y. (1977). *Phys. Rev. B*, **15**, 897-900.

MRSTIK, R., TONG, S. Y., KAPLAN, R. & GANGULY, A. K. (1975). *Solid State Commun.* **17**, 755-758.

NEAVE, J. H., JOYCE, B. A., DOBSON, P. J. & NORTON, N. (1983). *Appl. Phys.* A**31**, 1-8.

PENG, L. M. & COWLEY, J. M. (1986). *Acta Cryst.* A**42**, 545-552.

PENG, L. M. & COWLEY, J. M. (1987). *J. Electron Microsc. Tech.* **6**, 43-53.

RADI, G. (1970). *Acta Cryst.* A**26**, 41-56.

SHANNON, M. D., EADES, J. A., MEICHLE, M. E. & TURNER, P. S. (1985). *Ultramicroscopy*, **16**, 175-192.

SHANNON, M. D., EADES, J. A., MEICHLE, M. E., TURNER, P. S. & BUXTON, B. F. (1984). *Phys. Rev. Lett.* **53**, 2125-2128.

SMITH, A. E. & LYNCH, D. F. (1987*a*). *J. Vac. Sci. Technol.* A**5**, 1262-1265.

SMITH, A. E. & LYNCH, D. F. (1987*b*). *Surf. Sci.* **184**, 189-197.

STEEDS, J. W. (1979). *Convergent-Beam Electron Diffraction.* In *Introduction to Analytical Electron Microscopy*, edited by J. J. HREN, J. I. GOLDSTEIN & D. C. JOY. New York: Plenum.

STEEDS, J. W., TATLOCK, G. J. & HAMPSON, J. (1973). *Nature (London)*, **241**, 435-439.

TAKAYANAGI, K., TANISHIRO, T., TAKAHASHI, S. & TAKAHASHI, M. (1985). *Surf. Sci.* **164**, 367-392.

TATLOCK, G. J. & STEEDS, J. W. (1973). *Nature (London) Phys. Sci.* **246**, 126-128.

TOURNARIE, M. (1962). *J. Phys. Soc. Jpn*, **17**, Suppl. BII, 98-100.

TRIGUNAYAT, G. C. & VERMA, A. R. (1976). *Polytypism and Stacking Faults in Crystals with Layer Structure.* In *Crystallography and Crystal Chemistry of Materials with Layered Structures*, edited by F. LEVY. Dordrecht: Reidel.

TURNER, P. S. & COWLEY, J. M. (1981). *Ultramicroscopy*, **6**, 125-138.

VOSS, R., LEHMPFUHL, G. & SMITH, P. J. (1980). *Z. Naturforsch. Teil A*, **35**, 973-984.

WELTON-COOK, M. R. & BERNDT, W. (1982). *J. Phys. C*, **15**, 5691-5710.

WYCKOFF, R. W. G. (1963). *Crystal Structures*, 2nd ed. New York: Interscience.

YAGI, K., TAKAYANAGI, K. & HONJO, G. (1982). In *Crystals: Growth, Properties and Applications*, edited by H. C. FREYHARDT, Vol. 7, pp. 47-74. Berlin: Springer.